Acta Cryst. (1990). A46, 187-194

Particle Size Distribution and X-ray Diffraction Peak Profiles in Supersaturated Solid Solutions

BY S. CICCARIELLO*

Dipartimento di Fisica G. Galilei dell'Università, Padova, I-35131 Italy

AND G. FAGHERAZZI AND A. BENEDETTI

Dipartimento di Chimica-Fisica dell'Università, Venezia, I-30123 Italy

(*Received* 14 *June* 1989; *accepted* 26 *September* 1989)

Abstract

An analytical approximation of the correlation function relevant to a collection of spherical particles is obtained starting from a peaked particle distribution and neglecting any interparticle correlation. The distribution depends on two parameters, Δ and D_0, respectively the total width of the peak and the position of its left end. The distribution is such that by an appropriate variable rescaling and a suitable choice of the parameter Δ/D_0, a very accurate analytical approximation is obtained for the correlation function relevant to the particle distribution predicted by Lifshitz & Slyozov [*J. Phys. Chem. Solids* (1961), **19**, 35-50] and by Wagner [*Z. Elektrochem.* (1961), **65**, 581-590] for advanced stages of phase-separation processes in supersaturated solid solutions. By a Fourier transformation, two simple analytical expressions are obtained for the corresponding SAXS and WAXS peak profiles. The characteristic feature of these is the presence, in the experimentally accessible region, of some oscillations in the SAXS Porod plot and in the latter generalization appropriate to WAXS peaks. The observation of these features in peak profiles, relevant to samples where a demixing process may have occurred, and the subsequent use of the functional expressions presented here should make the numerical analysis of experimental data easier and yield a more definite answer on the nature of the demixing process.

I. Introduction

The shape of the peak profiles of the X-radiation diffracted by a crystalline powder sample is determined by the size distribution of the constituent crystallites as well as by the disorder present in the latters' lattices. Nowadays, in fact, the corrections of the broadening effects due to the experimental apparatus can be carried out with suitable optimization procedures and an appropriate standard material. Combined efforts of many researchers have led to the development of software which, even with a personal computer, yields high-precision results.† By contrast, the separation of the contribution due to size effects from that due to lattice disorder is even less accurate even when a Fourier analysis is employed. To a large extent, in fact, the separation is a matter of assumptions on the different kinds of lattice disorder which can be present. An indirect method of obtaining a deeper insight into this problem is to neglect disorder effects and to analyse how sensible choices of the particle distributions modify the shape of peak profiles. The subsequent comparison with experimental data should yield an estimate of the importance of neglected disorder effects. This paper, as for others appearing over the past few years [see for instance Rao & Houska (1986)], follows this approach. Our attention‡ in fact will focus on the skewness (Granquist & Buhrman, 1975) of size distribution functions. We analyse in detail a distribution which approximates sensibly the ones that, according to the theory by Lifshitz & Slyozov (1961) and Wagner (1961) (abbreviated as LSW), result from the demixing processes taking place in supersaturated solid solutions. Glasses (Zarzycki, 1974) constitute a paramount example. Of course it would be interesting to find a microcrystalline system showing a crystallite size distribution equal to the LSW one. It is probable it could be obtained by crystallizing, in a controlled way, demixed glasses where the precipitate coarsening has undergone an Ostwald ripening process, since the latter for glass-in-glass phase separation yields LSW particle size distributions.

The plan of the paper is the following. In the next section (II) we shall recall the main theoretical definitions and results. Particular attention will be

* Present address (until October 1990): Laboratoire de Physique des Solides, Bâtiment 510, 91405 Orsay CEDEX, France.

† For a discussion of these topics we refer to Delhez, de Keijser & Mittemeijer (1982), de Keijser, Langford, Mittemeijer & Vogels (1983) and to Enzo, Fagherazzi, Benedetti & Polizzi (1988). See also the August 1989 issue of the *Australian Journal of Physics*.

‡ A brief summary (Fagherazzi, Ciccariello & Benedetti, 1988) of this paper was presented by one of us (GF) at the 11th European Crystallographic Meeting.

0108-7673/90/030187-08$03.00

payed to those results which follow from the recently highlighted analogy (Ciccariello, 1990) that exists between the theoretical analysis of a single wide-angle X-ray scattering (WAXS) peak and that used in small-angle X-ray (SAXS) scattering. In the third section we introduce our approximation of the particle distribution, which, according to the LSW theory, ought to be realized in the last stages of demixing processes inside glasses (Zarzycki, 1974). The analytical expression for the suggested approximation is such that one can obtain the analytical expressions both of the peak profile and of the sample correlation function. In the fourth section we approximate the latter expressions by Voigt functions in order to see if and where discrepancies arise. We find that these are particularly evident in the Porod plot of the intensity. A conclusive section summarizes the paper.

II. General theory

Let us briefly recall the main theoretical definitions as well as some general properties following from the invoked analogy with the SAXS theory. According to the standard notation of X-ray diffraction theory (Guinier, 1963), let $\mathbf{S}_{0r} \equiv \mathbf{S}_{out} - \mathbf{S}_{in} = h\mathbf{a}^* + k\mathbf{b}^* + l\mathbf{c}^*$ denote the Bragg reflexion relevant to the rth set of Miller indices hkl. The corresponding peak profile is given by

$$I_r(h) \equiv \int I[(h_{0r}+h)\hat{\mathbf{s}}_{0r} + \mathbf{h}_\perp]\, \mathrm{d}^2 h_\perp = \int_{-\infty}^{\infty} \exp(-iht)\gamma_r(t)\, \mathrm{d}t, \quad (1)$$

where $\hat{\mathbf{s}}_{0r}$ is the unit vector associated with $\mathbf{S}_{0r}$ and $h_{0r} = 2\pi S_{0r}$. $\gamma_r(t)$ is proportional to the probability density that if a stick of length t and direction $\hat{\mathbf{s}}_{0r}$ is tossed randomly its ends fall inside the filled region of the sample. For this reason, it will also be referred to as the oriented stick probability function (oSPF) (Ciccariello, 1985). If one denotes by $\rho_V(\mathbf{r})$ the function characteristic of the filled region of the sample, then

$$\gamma_r(t) = V^{-1} \int_{R^3} \rho_V(\mathbf{r}_1)\rho_V(\mathbf{r}_1 + t\hat{\mathbf{s}}_{0r})\, \mathrm{d}v_1. \quad (2)$$

Denoting by V_i the region occupied by the ith crystallite, one has

$$\rho_V(\mathbf{r}) = \sum_i \rho_{V_i}(\mathbf{r}) \quad (3)$$

and (2) becomes

$$\gamma_r(t) = \sum_i (V_i/V) \int_{R^3} \rho_{V_i}(\mathbf{r}_1)\rho_{V_i}(\mathbf{r}_1 + t\hat{\mathbf{s}}_{0r})\, \mathrm{d}v_1/V_i + \sum_{i \neq j} (1/V) \int_{R^3} \rho_{V_i}(\mathbf{r}_1)\rho_{V_j}(\mathbf{r}_1 + t\hat{\mathbf{s}}_{0r})\, \mathrm{d}v_1. \quad (4)$$

The second sum on the r.h.s. of (4) is usually neglected on the basis that it should be small and structureless when particles are randomly distributed. For polydisperse systems of single-shape particles, the first sum can be converted into the integral

$$\gamma_r(t) = \int \mathrm{d}\Omega \int_0^\infty V(D)\pi(D, \Omega)\gamma_r(t, D, \Omega)\, \mathrm{d}D/V. \quad (5)$$

Here $V(D)$ is the volume of the particle having size D, $\pi(D, \Omega)$ is the number density of particles having a particular orientation ($\equiv \Omega$)* with respect to $\hat{\mathbf{s}}_{0r}$ and size D. Finally, $\gamma_r(t, D, \Omega)$ is the oSPF of the specified particle and it is obtained from (2), provided we interpret ρ_V here as the function characteristic of the spatial set occupied by the particle and V as the volume of the latter. Equation (2) implies that $\gamma_r(0, D, \Omega) = 1$ and $\gamma_r(0) = 1$ and thus the particle distribution function has to obey the normalization condition

$$V^{-1} \int \mathrm{d}\Omega \int_0^\infty V(D)\pi(D, \Omega)\, \mathrm{d}D = 1. \quad (6a)$$

Consequently,

$$\Pi(D, \Omega) \equiv V^{-1} V(D)\pi(D, \Omega) \quad (6b)$$

$$\Pi(D) \equiv V^{-1} V(D) \int \pi(D, \Omega)\, \mathrm{d}\Omega \quad (6c)$$

are true probability densities.

From (1) and a well known property of the Fourier transform, the behaviour of the peak profile $I(h)$† at small (large) h's reflects the behaviour of $\gamma(t)$ at large (small) t's. If one assumes that $\Pi(D, \Omega)$ decreases sufficiently fast at large D's and that it is a C^2 function in $[0, \infty)$, *i.e.* a continuous doubly differentiable function, then many properties of $\gamma(t, D, \Omega)$ hold true also for $\gamma(t)$. For this reason let us briefly recall some general properties of $\gamma(t, D, \Omega)$, which follow essentially from its geometrical meaning. One knows that:

(i) $\gamma(t, D, \Omega)$ is a non-negative even function with respect to t and has a t support not exceeding $2D$;

(ii) its first t derivative evaluated at the origin, *i.e.* $\gamma_r'(0, D, \Omega)$, is proportional to the area [$\equiv S_r(D)$] of the projection of the particle surface on a plane orthogonal to $\hat{\mathbf{s}}_{0r}$. More definitely, one has $\gamma'(0, D, \Omega) = -S_r(D)/V$ (Ciccariello, 1990);

(iii) for convex particles, $\gamma_r''(t, D, \Omega)$ is a non-negative quantity since, after multiplication by t, it represents the volume fraction of the particle relevant to a diameter length lying between t and $t + \mathrm{d}t$ and parallel to $\hat{\mathbf{s}}_{0r}$ (Guinier, 1963). One can also say that $t\gamma_r''(t, D, \Omega)$ is the probability density that a stick of length t, parallel to $\hat{\mathbf{s}}_{0r}$, has both its ends on the particle boundary;

(iv) $\gamma_r''(0, D, \Omega)$, being related to the existence of edges and of contact points, represents the angularity of the particle and one can show that the latter is a non-negative quantity;

* Ω represents the set of variables required for specifying the orientation of a particle, for instance the set of Euler angles.

† From now on we shall omit the index r when it is not necessary.

(v) $\gamma_r'(t, D, \Omega)$ has finite discontinuities for those t values such that a translation of the particle by $t\hat{\mathbf{s}}_{0r}$ yields a tangency of the two boundaries on a finite area set;

(vi) similarly, finite discontinuities arise in $\gamma_r''(t, D, \Omega)$ for those t values such that the translation of the particle by $t\hat{\mathbf{s}}_{0r}$ leads either to a tangency of a finite-length subset of the edges with the original particle surface or to a tangency condition at a regular point of the boundary with the tangent plane orthogonal to $\hat{\mathbf{s}}_{0r}$.

When the assumption previously made for $\Pi(D, \Omega)$ is fulfilled, properties (i)-(iv) also hold true for $\gamma(t)$. In particular, $\gamma'(0)$ and $\gamma''(0)$ will represent the average of the crystallite projected surface areas and angularities, respectively. On the contrary, properties (v)-(vi) are washed out by the average (5), but for the case of a δ-like distribution of particles. All these properties can be observed stemming directly from the measured peak profile $I(h)$, at least in principle. In fact, from (1) and (5), it follows immediately that

$$I(h) = \int \mathrm{d}\Omega \int_0^\infty \Pi(D, \Omega) I(h, D, \Omega)\, \mathrm{d}D \qquad (7)$$

so that $I(h)$ is the average of the crystallite peak profiles defined by

$$I(h, D, \Omega) = \int_{-\infty}^{\infty} \exp(-iht)\gamma_r(t, D, \Omega)\, \mathrm{d}t = 2\int_0^\infty \cos(ht)\gamma_r(t, D, \Omega)\, \mathrm{d}t. \qquad (8)$$

Property (ii) implies that, at very large h's, $I(h) \simeq 2\mathscr{S}h^{-2}$, where $\mathscr{S} = S/V$ and S is the average of quantities $S(D)$, *i.e.* the area of the crystallite surface projected along the direction $\hat{\mathbf{s}}_{0r}$. Conditions (i), (ii) and (iii) ensure that one can directly obtain the second derivative of the correlation function from the relation

$$\gamma''(t) = (1/\pi)\int_0^\infty [2\mathscr{S} - h^2 I(h)] \cos(ht)\, \mathrm{d}h. \qquad (9)$$

One should note that this relation, evaluated at $t = 0$, represents the WAXS modification of the Porod sum rule (Porod, 1965) yielding the angularity of a sample.

III. Approximation of the LSW peak profiles

Lifshitz & Slyozov (1961) and Wagner (1961) have performed an interesting theoretical analysis of demixing processes in supersaturated solutions, showing the universal behaviour of the leading approximation of the particle distribution function. In particular, they showed the existence of a critical radius [$\equiv r_c(t)$] (varying with the duration t of the demixing process), such that separated grains tend to disappear or to grow depending on whether their diameter D is smaller or greater than $2r_c(t)$. In this way it turns out that the final probability density of the grains in terms of their size is different from zero only in the interval $[0 < y = D/2r_c < 3/2]$, where its analytical expression is [Lifshitz & Slyozov (1961), see also Martin & Doherty (1976), § 4.5]

$$\Pi_{\mathrm{LSW}}(y) = \mathscr{C} y^2 (y+3)^{-7/3} (3/2 - y)^{-11/3} \times \exp[-(1 - 2y/3)^{-1}]. \qquad (10)$$

Here $y \equiv D/D_c$, with $D_c = 2r_c(t)$ and $\mathscr{C}$ is a normalization constant. We recall now that in the case of glasses we have strong experimental evidence that the separated particles have a spherical shape [Zarzycki (1974), see also Benedetti, Ciccariello & Fagherazzi (1988)]. The oSPF of a sphere, having diameter D, is given by

$$\gamma_{\mathrm{sph}}(t, D) = 1 - 3|t|/2D + |t|^3/2D^3 \quad |t| \le D \qquad (11)$$

and it is zero elsewhere. Then we can use (5) for evaluating the oSPF of a set of spheres obeying the LSW distribution given by (10). Firstly, instead of evaluating $\gamma(t)$ we find it more convenient to calculate its second-order derivative. On evaluation of the second-order derivative of (11), only the last term survives. This is proportional to $|t|D^{-3}$ and thus it cancels the corresponding $V(D)$ factor present in the integrand of (5). In this way one finds that*

$$\gamma_{\mathrm{LSW}}''(t) = \mathscr{C} t \int_t^\infty \Pi_{\mathrm{LSW}}(y)\, \mathrm{d}y. \qquad (12)$$

From this equation one immediately gets

$$\frac{\mathrm{d}}{\mathrm{d}t}\frac{\gamma_{\mathrm{LSW}}''(t)}{t} = -\mathscr{C}\Pi_{\mathrm{LSW}}(t). \qquad (13)$$

The functional dependence of (10) does not allow the integration of (12) in a closed analytical form. Thus the exact† peak profile of the LSW particle distribution can be obtained only in a numerical way. Since our main task is that of finding a recipe for isolating the main features of this kind of distribution we find it more convenient to approximate the LSW distribution by a function which has an analytical expression simple enough to carry through all

* Note that $\mathscr{C}$ represents the normalization constant appropriate to the particular equation where it appears. Therefore, although the symbol is the same, its explicit expression will generally depend on the considered equation. Moreover, in order to make the notation simpler, we shall confine ourselves to the region $t \ge 0$, since the oSPF's are even t functions.

† Modulo, of course, unavoidable numerical inaccuracies.

subsequent numerical calculations in an analytical way. For this reason we have chosen the following functional expressions

$$\Pi_*(\zeta,\delta)=\begin{cases}0 & \text{if } \zeta\le 1 \text{ or } 1+\delta\le\zeta\\ \mathscr{C}\left(\frac{2}{\delta}\right)\sin^2\left[\frac{\pi(\zeta-1)}{\delta}\right] & \\ & \text{if } 1\le\zeta\le 1+\delta.\end{cases}\quad(14)$$

One sees that $\Pi_*(\zeta,\delta)$ depends on two dimensionless variables: $\zeta\equiv D/D_0$ and $\delta\equiv\Delta/D_0$, where D_0 is a particular length. Also, $\Pi_*(\zeta,\delta)$ corresponds to a peak set at $\zeta=1+\delta/2$, with a width proportional to δ. The shape of the LSW distribution function, shown in Fig. 1, is similar to that of $\Pi_*(\zeta,\delta)$. We stress that the main reasons for choosing the functional expression (14) have been its fair accuracy in approximating the Π_{LSW} distribution, its analytical simplicity and the fact that $\Pi_*(\zeta,\delta)$ is a C^2 function throughout the closed half-line $[0\le\zeta\le\infty]$. This property is particularly important in order to preserve the first leading terms of the asymptotic expansion of the Fourier transform of γ'' (Ciccariello, Goodisman & Brumberger, 1988). Substituting (14) in (12), one gets

$$\gamma''_*(\zeta,\delta)=\begin{cases}\mathscr{C}\xi & \text{if } 0\le\xi\le 1\\ \mathscr{C}\xi\left\{1-\frac{(\zeta-1)}{\delta}+\left(\frac{1}{2\pi}\right)\sin\left[\frac{2\pi(\zeta-1)}{\delta}\right]\right\} & \\ & \text{if } 1\le\zeta\le 1+\delta\\ 0 & \text{if } 1+\delta\le\zeta.\end{cases}\quad(15)$$

The best agreement which can be realized between $\gamma''_*(\zeta,\delta)/\zeta$ and $\gamma''_{\mathrm{LSW}}(y)/y$ is shown in Fig. 1. It has been obtained by choosing for δ the value δ_{LSW} such that

$$\int_0^{1\cdot5}|\gamma''_*[\zeta(y),\delta]/\zeta(y)-\gamma''_{\mathrm{LSW}}(y)/y|^2\,dy,$$

where $\zeta(y)\equiv(1+\delta)y/1{\cdot}5$, turn out as small as possible. One should note that the peak of the particle distribution at $y\simeq 1$ does reflect now into a plateau in an interval next to the origin. Two further integrations yield the correlation function

$$\gamma_*(\zeta,\delta)=\begin{cases}1-\mathscr{C}\{[\frac{1}{2}+\delta(\delta+3)/6-a^{-2}]\zeta-\zeta^3/6\}\\ \qquad 0\le\zeta\le 1\\ \mathscr{C}[\{(\delta_+^4-\zeta^4)/12\delta-[\delta_+\zeta(\delta_+^2-\zeta^2)]/6\delta\\ \quad-[\delta\delta_+(\delta_+-\zeta)]/4\pi^2\}\\ \quad-1/2\pi(\xi\sin[a(\xi-1)]/a^2\\ \quad-2\{1-\cos[a(\xi-1)]\}/a^3)]\\ \qquad 1\le\zeta\le 1+\delta\\ 0\qquad 1+\delta\le\zeta,\end{cases}\quad(16)$$

where the following definitions have to be used

$$\delta_+\equiv 1+\delta\qquad a\equiv 2\pi/\delta\qquad(17a,b)$$

and the normalization constant $\mathscr{C}$, determined by the condition $\gamma_*(0^+,\delta)=1$, is

$$\mathscr{C}\equiv[\tfrac{1}{3}+\delta(\delta^2+4\delta+6)/12-\delta^2(2+\delta)/4\pi^2]^{-1}.\quad(17c)$$

One should note that the average specific surface is given by

$$\mathscr{S}=-\gamma'_*(0^+,\delta)=\mathscr{C}[\tfrac{1}{2}+\delta(\delta+3)/6-\delta^2/4\pi^2],\quad(18)$$

while the angularity $\gamma''_*(0^+,\delta)$ is null, since we are dealing with spherical particles. From (7), (8) and (16) it is rather straightforward to evaluate the intensity scattered by an assembly of spheres obeying the distribution (16). One finds†

$$I_*(h,\delta)=\frac{2\mathscr{S}}{h^2}+2\mathscr{C}\left\{\frac{1}{h^4}-\frac{a^2(\delta_+\cos h_+-\cos h)}{\delta h^4(h^2-a^2)}+\frac{2a^2(2h^2-a^2)(\sin h_+-\sin h)}{\delta h^5(h^2-a^2)^2}\right\}\quad(19)$$

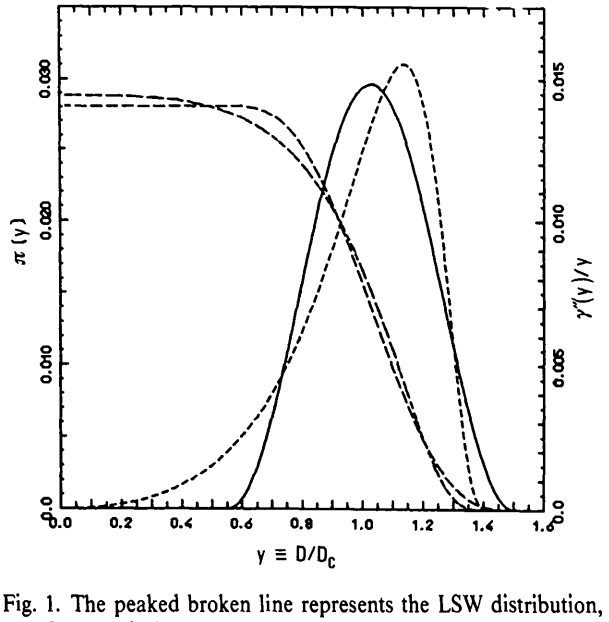

Fig. 1. The peaked broken line represents the LSW distribution, defined by (10). It refers to the left scale and the units are such that $\mathscr{C}=1$. The longer-dash curve, with a plateau on the left, represents $\gamma''_{\mathrm{LSW}}(y)/y$ obtained by the numerical evaluation of the integral on the r.h.s. of (12). The relevant scale is the right one. The short-dash curve represents the best L_2 approximation of $\gamma''_{\mathrm{LSW}}(y)/y$, obtained by a proper choice of the parameter δ, present in the function $\gamma''_*[\zeta(y),\delta]/\zeta(y)$ defined by (15) and by the rescaling $\zeta(y)=(1+\delta)y/1{\cdot}5$. In this way, we have obtained $\delta=1{\cdot}47$. The corresponding $\Pi_*[\zeta(y),\delta]$ distribution, representing the best approximation of the LSW one, is represented by the continuous curve. In passing we note that changes of parameter δ by less than 20% do not appreciably modify the overall picture.

† We note that throughout (19), (20) and (21), the h unit is D_0^{-1}. Moreover, our unit length has been set equal to D_0.

where $h_+ \equiv h\delta_+$ and $\mathscr{S}$, δ_+, a and $\mathscr{C}$ have been defined in (18), (17a–c), respectively. We note also that the peak intensity at the origin is

$$I_*(0, \delta) = \mathscr{C}\left\{\frac{\delta_+^5 - 1}{40\delta} - \frac{\delta(\delta_+^3 - 1)}{8\pi^2} + \frac{3\delta^4}{16\pi^4}\right\}. \quad (20)$$

Before concluding this section, we report the expression of the SAXS intensity, scattered by a collection of spherical particles obeying the distribution $\Pi_*(\zeta, \delta)$. Clearly, the correlation function is still given by (16), thus by Fourier transforming it is easy to evaluate the SAXS intensity $i_*(h, \delta)$. Actually this quantity turns out to be simply related to the WAXS peak profile, already evaluated. Starting in fact from the definition

$$i_*(h, \delta) = (4\pi/h) \int_0^\infty \zeta\gamma_*(\zeta, \delta) \sin(h\zeta)\, d\zeta,$$

one immediately gets

$$i_*(h, \delta) = -\frac{4\pi}{h}\frac{d}{dh}\int_0^\infty \gamma_*(\zeta, \delta)\cos(h\zeta)\, d\zeta$$

$$= -\frac{2\pi}{h}\frac{d}{dh} I_*(h, \delta). \quad (21)$$

To good accuracy, (19) also represents the peak profile of a LSW distribution of spherical particles.

IV. Numerical analysis

In Fig. 1 we have reported both the Π_{LSW} distribution and one of its best Π_* approximations. They are the peaked curves on the right. The two curves with a plateau on the left represent their integrals from the extreme right up to y. They are the functions $\gamma''_{LSW}(y)/y$ and $\gamma''_*(\zeta, \delta)/\zeta$, with $\zeta = (1+\delta)y/1{\cdot}5$ and $\delta = 1{\cdot}47$. The latter value resulted from requiring that the L_2 norm of the function $\gamma''_{LSW}(y)/y - \gamma''_*(\zeta, \delta)/\zeta$ turns out as small as possible. Two subsequent numerical integrations of $\gamma''_{LSW}(y)$ yield the numerical expression of $\gamma_{LSW}(y)$, represented by the continuous line in Fig. 2. The best fit, always in the L_2 sense, of this function by the $\gamma_*(\zeta, \delta)$ expression, given by (16), yielded for δ the value $1{\cdot}71 (\equiv \delta_{LSW})$.† The lower part of Fig 2 shows that the maximum difference between $\gamma_{LSW}(y)$ and $\gamma_*(\zeta, \delta_{LSW})$ is 2×10^{-4}. This fact and the properties

(a) $\gamma_*(\zeta, \delta)$ and $\gamma_{LSW}(y)$ have the same y support

(b) the derivatives $\gamma_*^{(n)}(\zeta, \delta)$'s are continuous throughout the positive ζ axis up to $n = 4$

(c) $\gamma'_*(0, \delta_{LSW}) - \gamma'_{LSW}(0) = 10^{-4}$†

(d) $\gamma''_*(0, \delta_{LSW}) = \gamma''_{LSW}(0) = 0$

allow us to conclude that the peak profile resulting from (19), with $\delta = \delta_{LSW}$, can be confidently identified with the LSW exact one. The profile is represented by the continuous curve in Fig. 3. It is now natural to look for the most typical feature of this profile. To this aim we have analysed it by standard WAXS techniques. In fact we have best-fitted the LSW correlation function $[\gamma_{LSW}(y)]$ by a function defined as

$$\nu_{gI}(y; \alpha, \beta) \equiv \exp(-\alpha|y| - \beta^2 y^2), \quad (22)$$

where α and β are adjustable parameters. We remark that (22) is the Fourier transform of the so-called Voigt function which is commonly believed to be one of the most reliable functional parametrizations in order to best fit intensity peak profiles (Delhez, de Keijser & Mittemeijer, 1982; Benedetti, Fagherazzi, Enzo & Battagliarin, 1988). We have considered two cases:

† The difference of this value from the former one is simply a consequence of the fact that the region where the relevant minima occur is rather flat, so that any choice of δ in the range 1·2, 1·9 does not appreciably modify the overall picture.

† In the numerical evaluation of the integral expression of $\gamma_{LSW}(y)$, we have used a Δy step increment equal to 10^{-4}. Consequently, we can ignore the former difference.

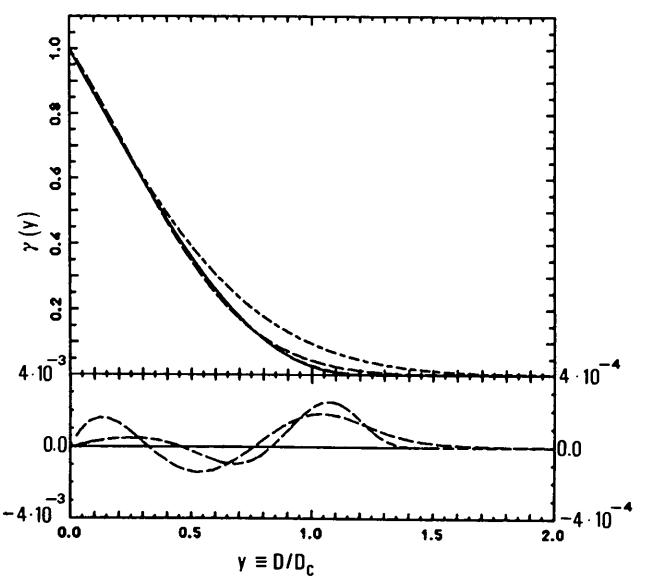

Fig. 2. In the upper part of the figure, the continuous curve shows the correlation function $\gamma_{LSW}(y)$ obtained by three subsequent numerical integrations of (10). The dash-dot curve represents ν^{II}_{gI}, *i.e.* the best γ_{LSW} approximation obtained by using a Voigt function $[\nu_{gI}(y; \alpha, \beta)]$ and requiring that the corresponding α and β values are the ones yielding the specific surface and the angularity appropriate to the LSW distribution. The broken line represents ν^{I}_{gI}, the best L_2 approximation of γ_{LSW} obtained with a Voigt function. The best L_2 approximation with a $\gamma_*(y, \delta)$ function is also shown. In order to appreciate the differences, in the lower part of the figure we plot the corresponding difference functions $\gamma_{LSW}(y) - \nu^{I}_{gI}(y; \alpha, \beta)$ and $\gamma_{LSW}(y) - \gamma_*(y, \delta)$. They are the short-dash and long-dash-short-dash lines, respectively, while the appropriate vertical scales are 10^{-3} and 10^{-4}.

(I) parameters α and β have been determined by minimizing the L_2 norm of $(\gamma_{LSW}-\nu_{gt})$. From this $\alpha^{(I)}=1{\cdot}11$ and $\beta^{(I)}=1{\cdot}42$. The corresponding Voigt approximation will be denoted as $\nu_{gt}^{(I)}$;

(II) we have required that the values at the origin of the first two derivatives of the required Voigt approximation are equal to those of γ_{LSW}, namely

$$\gamma'_{gt}(0)=-\alpha=\gamma'_{LSW}(0)=-1{\cdot}39 \qquad (23a)$$

$$\gamma''_{gt}(0)=\alpha^2-2\beta^2=\gamma''_{LSW}(0)=0. \qquad (23b)$$

The resulting approximation will be denoted by $\nu_{gt}^{(II)}(y)$.

Fig. 2 shows that the agreement achieved in the first case is better than in the second one. This conclusion, however, is rather rash, since we have to look also at the corresponding peak profiles. To this aim we have to Fourier transform (22). According to the general analysis of van de Hulst & Reesinck (1947), the FT can be fairly approximated by

$$\eta/(1+h^2/\bar{\beta}^2)+(1-\eta)\exp(-\ln 2h^2/\bar{\beta}^2).$$

The first and second contributions are usually referred to as Lorentzian and Gaussian, while the parameter $\eta_g\equiv 1-\eta$ is called the Gaussian content of the Voigt function (22). Kielkopf (1973) has clearly expounded how to calculate $\bar{\beta}$ and η starting from the parameters α and β present in (22). The resulting peak profiles $I^{(I)}(q)$ and $I^{(II)}(q)$ $(q\equiv hD_c)$, relevant to the above two cases, are represented respectively by the short-dash and long-dash curves of Fig. 3. One sees that at very large q's the profile $I^{(II)}(q)$ is much closer to the real one than $I^{(I)}(q)$. This result is an obvious consequence of (23a), which guarantees that the leading asymptotic term of $I^{(II)}(q)$ is equal to that of $I_{LSW}(q)$. By contrast, neither this condition nor the one relevant to a null angularity, *i.e.* (23b), are fulfilled in case I. These two aspects are evident from Fig. 4: (a) at large q's the plateau of the curve $q^2I^{(I)}(q)$ (short-dash line) lies definitely below that of the continuous curve and (b) the curve $q^2I^{(I)}(q)$ lies mostly above its horizontal asymptotic line [so as to have a (meaningless) positive angularity]. In conclusion, after having taken into accout also the fact that, for normalization reasons, $q^2I^{(II)}(q)$ must be suitably scaled so that it superimposes on the continuous line at very large q's, one sees that the profile $I^{(I)}(q)$ is more accurate than $I^{(II)}(q)$ only in the region $q<5$, while at larger q's the opposite becomes true. As a matter of fact, it is advisable that the analysis does not depend too much upon the asymptotic behaviour. Luckily, Fig. 4 offers a feature that can be considered typical of the LSW peak and it is present in a region which is not yet too much asymptotic. We are referring

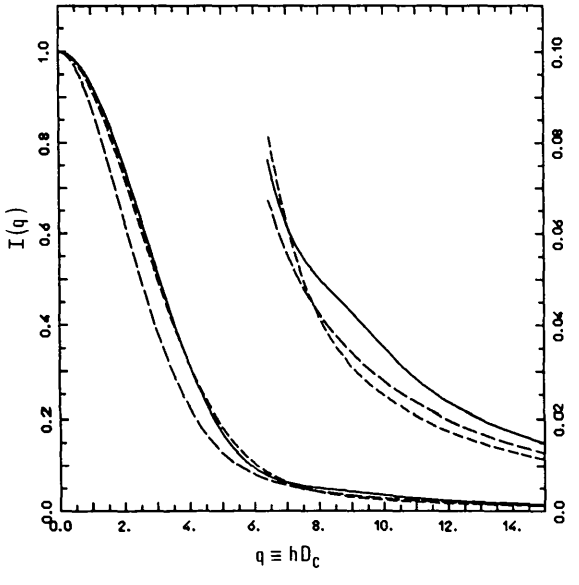

Fig. 3. The continuous line represents the intensity peak profile relevant to the best γ_* approximation of γ_{LSW}. The two broken lines, respectively with the short and long dashes, are the two best Voigt-function approximations: ν_{gt}^{I} and ν_{gt}^{II}, defined in § IV, of the LSW peak profile. The curves on the right refer to the right scale and allow one to appreciate the small differences present in the tail region.

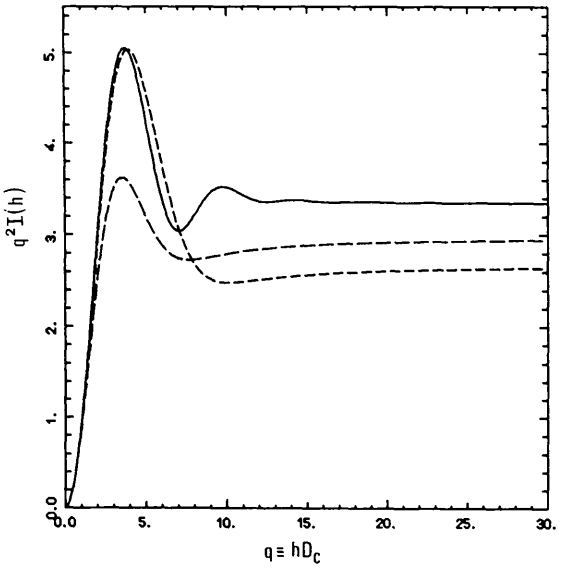

Fig. 4. The curves represent the Porod plots relevant to the WAXS profiles discussed in Fig. 3. The existence of a plateau is evident for the three curves. However, one should note that $I_*(h, \delta_{LSW})$ and hence also the LSW profile show, next to the main peak, a further appreciable oscillation, which is not present in the Voigt profiles. Therefore, a good resolution of experimental peaks in this region would easily allow one safely to estimate the necessity of using the γ_* distribution. Finally, we note that the different height of the ν_{gt}^{II} plateau, with respect to that of the γ_* curve, is simply a consequence of the fact that we are using the intensities normalized as in Fig. 3. A quantitative Porod plot, in fact, requires that the intensity be normalized so as to have $\int_0^\infty I(h)\,dh=\pi$, as follows from (8) and from the condition $\gamma_r(0)=1$. On the contrary, from this figure it is evident that the Porod invariant, *i.e.* the value of the former integral for the ν_{gt}^{II} approximation is higher than the LSW one.

to the presence of a second observable peak in the region $q \simeq 10$. Therefore, the observation of such a feature in the Porod plot of a WAXS peak profile can be a good reason for using (19) in fitting the profile.

We note also that the use of this function has also some important implications concerning the so-called volume-fraction weighted distribution (v.f.w.d.), defined as $\Pi_v(y) = \mathscr{C} y \gamma''(y)$ (Guinier, 1963). The continuous line of Fig. 5 represents the v.f.w.d. $\Pi_{v,\mathrm{LSW}}(y)$ while the close short-long-dash curve represents $\Pi_{v,*}(\zeta, \delta_{\mathrm{LSW}})$. The remaining two curves are relevant to the Voigt approximations considered. (The one with shorter dashes refers to $\nu_{gt}^{(\mathrm{II})}$.) The limitations are evident: neither $\nu_{gt}^{(\mathrm{I})}$ nor $\nu_{gt}^{(\mathrm{II})}$ are able to reproduce the sharp decrease of the real distribution. In fact, when they are forced to do that as in the $\nu_{gt}^{(\mathrm{I})}$ case, one finds a negative population for particles with smaller diameters. Fig. 6 shows the SAXS intensities relevant to the Π_* distributions characterized by the following δ values: δ_{LSW} (continuous line) and 0·1 (broken line). The comparison with Fig. 4 shows that in the LSW case the oscillations in the SAXS profile are wider than in the WAXS one. In both cases, however, their amplitude decreases fast with q. By contrast, in the case $\delta = 0{\cdot}1$, the oscillations still remain rather wide, although the washing effect due to the small polydispersity can be seen from the fact that the intensity no longer becomes zero at the relative minima.†

V. Concluding remarks

The peak profile for a distribution of spherical particles obeying the distribution law given by (14) has been explicitly evaluated under the assumption that the interparticle interference can be neglected. The former distribution, depending on two parameters D_0 and δ, is such that by fixing the latter's value at 1·71, one gets a very accurate approximation of the LSW particle distribution and consequently of its peak profile. The characteristic feature of this intensity is the presence of two peaks in its WAXS Porod plot,

† At small q's, in fact, the distribution can be looked upon as a monodisperse one, while the expected absence of the oscillatory terms decreasing as h^{-4} will become really effective only when q is sufficiently large for the related quantity $q\delta$ to satisfy the condition $q\delta > 2\pi$, according to the empirical criterion for the onset of the relevant asymptotic behaviour.

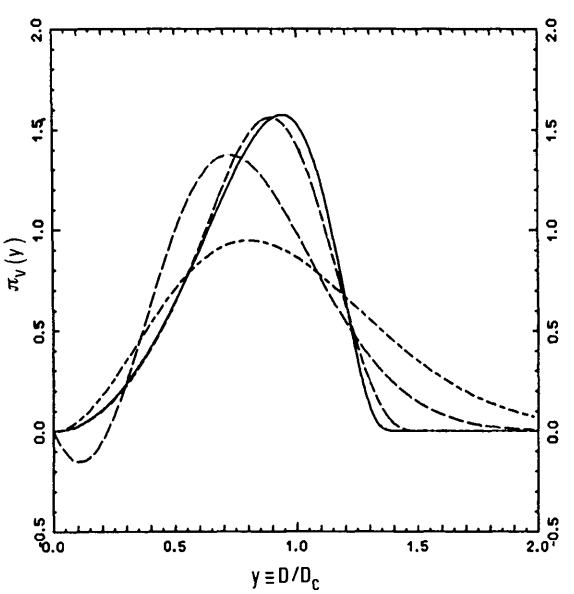

Fig. 5. The volume-weighted distributions of the particles for the ideal LSW case (continuous curve), for the γ_* approximation (– – – –), for the ν_{gt}^{I} (— — — —) and for the ν_{gt}^{II} (– – –) cases are represented. One should note the rather abrupt way the LSW volume distribution goes to zero as $y \to 1{\cdot}5$. By contrast, distributions usually obtained by Lorentzian approximations show a much longer tail, revealing opposite skewness in the distribution (Granquist & Buhrman, 1975; Fagherazzi *et al.*, 1988). This effect survives also in the figure, although the ν_{gt}^{I} have been determined by a best-fit procedure. This fact shows that Voigt functions are unable to describe these skewed distributions. Forcing the choice in order to get a better agreement, one ends up with a unphysical solution. In fact, the distribution relevant to the ν_{gt}^{I} function is negative at small y's.

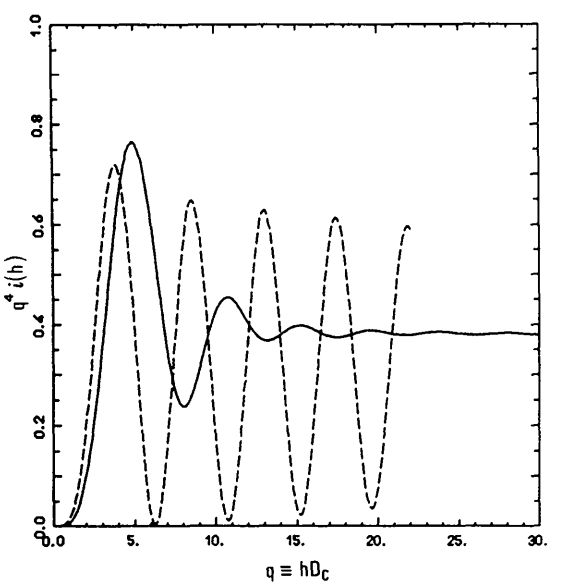

Fig. 6. The continuous curve represents the Porod plot of the SAXS intensity scattered by the Π_* distribution of spherical particles, characterized by the LSW value $\delta = 1{\cdot}71$. Thus it represents also to a fairly good approximation the SAXS intensity of a LSW distribution of spherical particles. Since the value of the parameter δ is rather large, one sees that the oscillations are considerably washed out, although they are larger than around WAXS peaks. (See Fig. 4.) By contrast, the broken line represents the intensity scattered by the more peaked Π_* distribution, characterized by the value $\delta = 0{\cdot}1$. The resulting Porod plot is quite similar to that of a spherical particle with radius r_c.

located in the region $3 < q < 10$. Therefore, the presence of this feature in observed peak profiles, resulting from samples where a demixing process has probably occurred, will make the use of the aforesaid analytical expression quite advantageous. From a numerical point of view, in fact, the use of (19) is only slightly more complicated than that of pseudo-Voigt functions. Besides, with $\delta = \delta_{LSW}$, it involves only one parameter, D_0 or equivalently D_c. This result is interesting for three reasons: (*a*) it makes it possible to test whether the conditions underlying the LSW theory are met or not, directly using WAXS results; (*b*) one could use SAXS experimental results for testing the applicability of the LSW model. In the affirmative case, one knows the ideal WAXS profiles. Thus any deviation ought to be ascribed to disorder effects; (*c*) with δ as a free parameter, one has another simple expression for fitting peak profiles. If it turns out that the overall agreement is better than that obtained by using Voigt functions, one would find a v.f.w.d. skewed in a direction opposite to the ones so far observed.

Financial support from the Italian Ministry of University and Scientific Research through 40% funds is acknowledged.

References

BENEDETTI, A., CICCARIELLO, S. & FAGHERAZZI, G. (1988). *Phys. Chem. Glasses*, **29**, 173-178.

BENEDETTI, A., FAGHERAZZI, G., ENZO, S. & BATTAGLIARIN, M. (1988). *J. Appl. Cryst.* **21**, 543-549.

CICCARIELLO, S. (1985). *Acta Cryst.* A**41**, 560-568.

CICCARIELLO, S. (1990). *Acta Cryst.* A**46**, 175-186.

CICCARIELLO, S., GOODISMAN, J. & BRUMBERGER, H. (1988). *J. Appl. Cryst.* **21**, 117-128.

DELHEZ, R., DE KEIJSER, TH. H. & MITTEMEIJER, E. J. (1982). *Z. Anal. Chem.* **312**, 1-16.

ENZO, S., FAGHERAZZI, G., BENEDETTI, A. & POLIZZI, S. (1988). *J. Appl. Cryst.* **21**, 536-542.

FAGHERAZZI, G., CICCARIELLO, S. & BENEDETTI, A. (1988). *Z. Kristallogr.* **185**, 694.

GRANQUIST, C. G. & BUHRMAN, R. A. (1975). *J. Catal.* **42**, 477-479.

GUINIER, A. (1963). *X-ray Diffraction.* San Francisco: Freeman.

HULST, H. C. VAN DE & REESINCK, J. J. M. (1947). *Astrophys. J.* **106**, 121-127.

KEIJSER, TH. H. DE, LANGFORD, J. I., MITTEMEIJER, E. J. & VOGELS, A. B. P. (1983). *J. Appl. Cryst.* **15**, 308-314.

KIELKOPF, J. F. (1973). *J. Opt. Soc. Am.* **63**, 987-995.

LIFSHITZ, I. M. & SLYOZOV, V. V. (1961). *J. Phys. Chem. Solids*, **19**, 35-50.

MARTIN, J. W. & DOHERTY, R. D. (1976). *Stability of Microstructure in Metallic Systems.* Cambridge Univ. Press.

POROD, G. (1965). *Small-Angle X-ray Scattering*, edited by H. BRUMBERGER, pp. 1-16. New York: Wiley.

RAO, S. & HOUSKA, C. R. (1986). *Acta Cryst.* A**42**, 6-13.

WAGNER, C. (1961). *Z. Elektrochem.* **65**, 581-590.

ZARZYCKI, J. (1974). *J. Appl. Cryst.* **7**, 200-207.

Acta Cryst. (1990). A**46**, 194-201

BYPASS: an Effective Method for the Refinement of Crystal Structures Containing Disordered Solvent Regions

BY P. VAN DER SLUIS AND A. L. SPEK*

Laboratorium voor Kristal- en Structuurchemie, Rijksuniversiteit Utrecht, Transitorium 3, *Padualaan* 8, 3584 *CH Utrecht, The Netherlands*

(*Received* 14 *April* 1989; *accepted* 26 *September* 1989)

Abstract

A method is described for the least-squares refinement of the atomic parameters of the ordered part of a crystal structure in the presence of disordered solvent areas. Potential solvent regions are identified automatically. The contribution of the observed contents to the total structure factor is calculated *via* a discrete Fourier transformation, and incorporated in a further least-squares refinement of the ordered part of the structure. The procedure is iterated a few times to convergence. It is found that this mixed discrete-atom and continuous solvent-area model refinement approach greatly improves the quality of discrete atomic parameters, *i.e.* the geometry and the e.s.d.'s. An electron count over the solvent region in the final difference electron-density map provides a convenient estimate for the number of solvent molecules present in the unit cell. The application of the method to four structures is described.

Introduction

The completion of an otherwise successful structure determination is frequently hampered by the presence of statically or dynamically disordered solvent of crystallization filling voids in the structure (*e.g.* Raston & White, 1976; Read & James, 1980). The problem of disordered solvent areas is very common in protein crystallography. Several methods are used

* Author to whom correspondence should be addressed.

0108-7673/90/030194-08$03.00